

The topologies of the charge densities in Zr and Ru

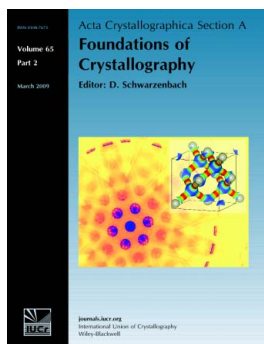
Travis E. Jones and Mark E. Eberhart

Acta Cryst. (2009). **A65**, 141–144

Copyright © International Union of Crystallography

Author(s) of this paper may load this reprint on their own web site or institutional repository provided that this cover page is retained. Republication of this article or its storage in electronic databases other than as specified above is not permitted without prior permission in writing from the IUCr.

For further information see <http://journals.iucr.org/services/authorrights.html>



Acta Crystallographica Section A: Foundations of Crystallography covers theoretical and fundamental aspects of the structure of matter. The journal is the prime forum for research in diffraction physics and the theory of crystallographic structure determination by diffraction methods using X-rays, neutrons and electrons. The structures include periodic and aperiodic crystals, and non-periodic disordered materials, and the corresponding Bragg, satellite and diffuse scattering, thermal motion and symmetry aspects. Spatial resolutions range from the subatomic domain in charge-density studies to nanodimensional imperfections such as dislocations and twin walls. The chemistry encompasses metals, alloys, and inorganic, organic and biological materials. Structure prediction and properties such as the theory of phase transformations are also covered.

Crystallography Journals **Online** is available from journals.iucr.org

The topologies of the charge densities in Zr and Ru

Travis E. Jones* and Mark E. Eberhart

Molecular Theory Group, Colorado School of Mines, Golden, Colorado 80401, USA.

Correspondence e-mail: trjones@mines.edu

Received 22 October 2008

Accepted 6 January 2009

We report on the atomic scale phenomena responsible for the variation of oxygen solubility in Zr and Ru. First-principles calculations reveal that the topologies of the charge densities in these hexagonal close-packed metals are distinct. Neither element was found to possess the topology of the prototype, Mg. There are 12 bond paths terminating at each Ru atom. These are the bonds between nearest neighbors. Only five bond paths terminate at each Zr atom and the Zr atoms are not bound to one another. Instead, they are bonded through non-nuclear maxima. As a result, channels of low charge density that can accommodate oxygen anions are present in Zr.

© 2009 International Union of Crystallography

Printed in Singapore – all rights reserved

1. Introduction

Oxygen dissolves interstitially to the octahedral holes of hexagonal close-packed (h.c.p.) metals. However, the extent to which it dissolves, its solubility, is remarkably variable. The Group IV metals (Ti, Zr, Hf) are characterized by appreciable oxygen solubility of the order of 20 at.%. In contrast, oxygen is nearly insoluble in the Group VIII h.c.p. metals (Ru, Os). The underlying structure responsible for this remarkable variation arises from the different charge-density topologies of these metals.

The topological theory of molecular structure, the ‘atoms in molecules’ (AIM) theory, was first articulated by Bader. This theory has been applied to a variety of crystalline systems (Bader, 1990; Zou & Bader, 1994). The first application of AIM theory to the solid state revealed that there are no second-neighbor bonds in face-centered cubic (f.c.c.) transition metals (Eberhart *et al.*, 1991). Subsequent studies have supported that observation (Eberhart *et al.*, 1992; Kioussis *et al.*, 2002), and have also been extended to show that nonmagnetic body-centered cubic (b.c.c.) transition metals possess only first-neighbor bonds (Eberhart, 1996a). However, there is no reason why second-neighbor bonds should not exist. As Zou pointed out, the only symmetry requirement is that the non-nuclear critical points lie on the Wigner–Seitz cell (Zou & Bader, 1994). Moreover, a more recent study of f.c.c. and b.c.c. iron has shown that second-neighbor bonds are present in magnetic transition metals (Jones, Eberhart & Clougherty, 2008).

This ability to unambiguously define bonds has made AIM theory a useful tool for the investigation of ‘bonding’ in materials ranging from high-temperature alloys to biological systems. These investigations have yielded interesting results. The geometry of the charge density at bond points was found to correlate with the single-crystal elastic moduli in f.c.c. and b.c.c. transition metals (Eberhart, 1996a,b). Second-neighbor bond paths were found in B2 ionic crystals (Luaña *et al.*, 1997)

and transition-metal aluminides (Eberhart & Giamei, 1998), with the magnitude of the latter correlating to failure properties (Eberhart, 2001). Second-neighbor bond paths were also found in iron, where a well known magnetic phase change was shown to be a topological phase transition (Jones, Eberhart & Clougherty, 2008). Other studies have used the geometry of the charge density at bond points to offer first-principles explanations of the anomalous behavior of iridium under shear (Kioussis *et al.*, 2002), as well as the motion of Ta and Mo screw dislocation cores (Jones, Eberhart, Clougherty & Woodward, 2008).

One of the attractive features of AIM theory is its reliance on the charge density, a quantum-mechanical observable, which can be measured *via* X-ray diffraction techniques and can be calculated by first-principle methods. Numerous studies have been performed in an effort to compare the topologies found by these two approaches. In an overwhelming majority of cases, the experimental and theoretical topologies are identical (Koritsanszky & Coppens, 2001). Furthermore, as both techniques have advanced, the values of the charge density measured by the two approaches have converged (Farrugia & Evans, 2005; Arnold *et al.*, 2000). We expect this trend to continue and in the near future there will be negligible difference between calculated and measured charge densities. This fact can be used to great effect in the fields of materials science and condensed matter physics, where accurate density functional theory (DFT) calculations have become routine. Given this fact, it becomes plausible to use first-principle methods to uncover structure–property relationships, which are then subject to experimental confirmation.

Incorporating first-principles methods into the discovery process could accelerate the pace of scientific understanding and technological advance. As an example, here we compare the topologies of two h.c.p. elements, Zr and Ru, by way of first-principles calculations. Surprisingly, while the crystal structure of the two metals is identical, we find that their

topologies, and hence their structures, are not. The Group IV metal, Zr, is characterized by five bond paths per atom and Ru by 12. The unusual and unexpected topology of Zr creates channels of low charge density, which we argue are the cause of the metal's high oxygen solubility.

The relationship between the topology of the charge density and many properties of materials can be rationalized from the Hohenberg–Kohn theorem, which states that a system's ground-state properties are a consequence of its charge density, a scalar field denoted here as $\rho(\mathbf{r})$ (Hohenberg & Kohn, 1964). Bader noted that the essence of a molecule's structure must be contained within the topology of $\rho(\mathbf{r})$. The topology of a scalar field, in this case $\rho(\mathbf{r})$, is given in terms of its critical points (CPs), which are the zeros of the gradient of this field. There are four kinds of CP in a three-dimensional space: a local minimum, a local maximum and two kinds of saddlepoint. These CPs are denoted by an index, which is the number of positive curvatures minus the number of negative curvatures. For example, a minimum CP has positive curvature in three orthogonal directions; therefore it is called a (3, 3) CP. The first number is simply the number of dimensions of the space, and the second number is the net number of positive curvatures. A maximum is denoted by (3, -3), since all three curvatures are negative. A saddlepoint with two of the three curvatures negative is denoted (3, -1), while the other saddlepoint is a (3, 1) CP.

2. Methods

In this study, charge densities were calculated using the *Vienna ab-initio Simulation Package (VASP)* version 4.6 (Kresse & Furthmüller, 1996), which is based on the projector augmented wave method (PAW) (Kresse & Joubert, 1999). A Γ -centered grid was employed to retain full hexagonal symmetry. The calculations reported here were performed using a grid of $25 \times 25 \times 15$ k points for both metals. The PAW

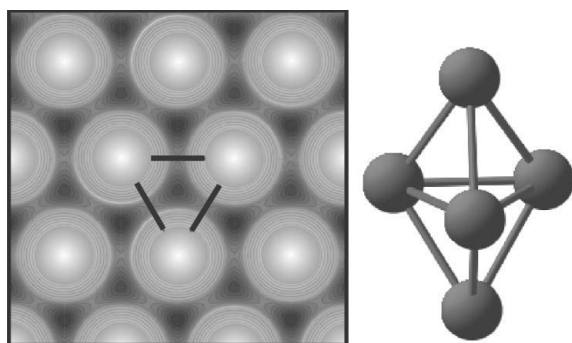


Figure 1

Contour plot of the total charge density in the basal plane of Ru. The light areas are regions of high charge density and the dark areas are regions of low charge density. Each Ru atom is bound to its six nearest neighbors in the plane, which can be recognized by the bond points, the saddles in the contour plot. Three of the bond paths have been drawn in as lines forming the face of adjoining tetrahedral holes, as shown on the right. For the adjacent octahedral holes the region of low charge density is less extended than for Zr (see Fig. 2).

potentials were used for both Zr and Ru, and the kinetic energy cutoffs used were 193.3 eV for Zr and 266.6 eV for Ru. A total of 6144 ($16 \times 16 \times 24$) plane waves were employed in the Zr calculations and 4704 ($14 \times 14 \times 24$) plane waves were used in the Ru calculations. The Perdew–Wang generalized gradient corrections (Perdew *et al.*, 1992) were included along with the Vosko–Wilk–Nusair interpolation (Vosko *et al.*, 1980) of the correlation part of the exchange–correlation functional. These calculations were performed using the published lattice constants (Villars & Calvert, 1985), as well as a variety of others within $\pm 10\%$ of these values. The topologies, calculated using *Tecplot* (Tecplot, 2008), were not affected by changes in the lattice constants. To check the stability of these structures, we also calculated the vibrational frequencies at the published lattice constants. There were no negative or imaginary frequencies.

3. Results

Calculations performed on nonmagnetic monotonic b.c.c. (f.c.c.) transition metals show that the ground-state total charge densities share the same topology as the prototype structure, W (Cu) (Eberhart, 1996*a,b*; Jones, Eberhart & Clougherty, 2008). Each atom has 8 (12) bond paths to its nearest-neighbor atoms. In these systems it is the geometry of the charge density around the CPs that leads to differences in, for example, single-crystal shear moduli (Eberhart, 1996*b*). However, the same trend is not observed in the h.c.p. metals. Neither Zr nor Ru have the topology of the prototype, Mg. To facilitate the visualization of the three-dimensional bonding in the two transition metals, we begin with an examination of a two-dimensional slice, in particular, a slice through a basal plane. Shown in Figs. 1 and 2 are contour plots of the charge density in these planes. Here regions of low charge density are darker and the regions near the nucleus are shown as spheres.

As expected, the densities around the atomic nuclei are similar, although the regions between the atoms are quite

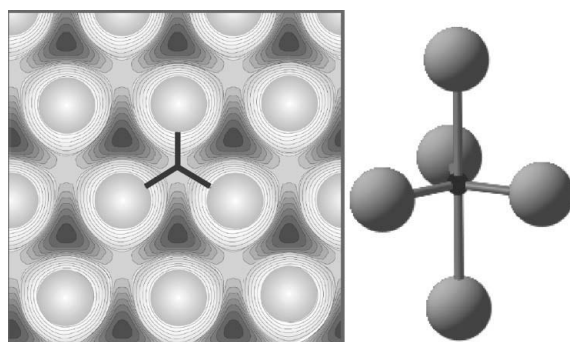


Figure 2

Contour plot of the total charge density in the basal plane of Zr. The shading is like that of Fig. 1. Here, however, each Zr atom is bound to three pseudo atoms in the plane. In effect this results in five Zr atoms being bound to one another through the tetrahedral hole, as shown on the right. The bonding through the tetrahedral holes produces regions of extremely low and extended charge-density minima centered on the octahedral holes.

different. On the one hand, there are six bond CPs, the saddlepoints, located on the boundaries between Ru atoms. From any one of these, the charge density increases in the direction of the atomic nuclei (positive curvature) and decreases in the directions tangential to the atomic spheres (negative curvature). The bond path is given by following the gradient of the charge density from a bond CP toward the bound atoms. Hence the bond paths in Ru (three are shown as lines) are straight with every atom in the basal plane bound to six other atoms in the same plane. In addition, each Ru atom is bound to the three nearest-neighbor atoms above and below the basal plane, giving rise to 12 nearest-neighbor bonds. The three-dimensional bonding around adjoining tetrahedral holes is depicted on the right-hand side of Fig. 1. This type of nearest-neighbor bonding, where the atoms are joined by a straight bond path, is typical for b.c.c. and f.c.c. transition metals (Eberhart, 1996*a,b*; Jones, Eberhart & Clougherty, 2008).

On the other hand, for Zr the bonding is quite different, with only three basal-plane bond paths originating from the face of adjoining tetrahedral holes and terminating at each atomic site (Fig. 2). While the bond paths can easily be identified, the topology near the point of intersection cannot, as the charge density is nearly flat in these regions (see Appendix A). However, the simplest topology that will give rise to this bonding pattern will have pseudo atoms, (3, -3) CPs, at the points of intersection. These pseudo atoms are bound to the five Zr atoms at the vertices of adjacent tetrahedral holes. In effect, h.c.p. Zr and h.c.p. Ru possess different structures. This is in contrast to the nonmagnetic f.c.c. and b.c.c. transition metals, which all share the same structure characterized by nearest-neighbor bond paths (Eberhart, 1996*a*). In f.c.c. and b.c.c. transition metals pseudo atoms are only present in magnetic systems. The spin minority density in high-spin f.c.c. Fe ($2.5 \mu_B$), for example, is characterized by bonding through pseudo atoms. In this case the pseudo atoms allow the f.c.c. Fe to possess a pseudo-b.c.c. topology by allowing each Fe atom to form eight σ -bonds directed towards the tetrahedral holes. This is due to the fact that d -orbitals reducing as T_{2g} vastly outnumber those reducing as E_g at moments in excess of $2.5 \mu_B$. As such, 12 bonds cannot be formed, as that would require both the T_{2g} and E_g representations (Jones, Eberhart & Clougherty, 2008). Such a change in topology due to an electron deficiency can also explain the pseudo atoms in h.c.p. Zr.

4. Discussion

The presence of five bond paths in Zr, as opposed to 12 in Ru, can be rationalized by way of directed valence. Each nuclear site sits in a D_{3h} environment, see Figs. 1 and 2. In this environment there are two symmetry-unique sets of σ -bonds: those in and those inclined to the basal plane. Six σ -bonds directed towards the nearest-neighbor atoms in the basal plane reduce as $\Gamma_{\sigma}^{\text{basal}} = A'_1 + A'_2 + 2E'$. Similarly, six σ -bonds directed towards the nearest-neighbor atoms above and below the basal plane reduce as $\Gamma_{\sigma}^{\text{inclined}} = A'_1 + E' + A'_2 + E''$. The

12 directed σ -bonds will transform as the sum $\Gamma_{\sigma}^{\text{total}} = \Gamma_{\sigma}^{\text{basal}} + \Gamma_{\sigma}^{\text{inclined}}$. For a central atom orbital to be available to form these 12 directed bonds, it must transform as one of the irreducible representations in $\Gamma_{\sigma}^{\text{total}}$. In a transition metal we must consider the s -, p - and d -orbitals. While s -orbitals always transform as the totally symmetric representation, the p -orbitals are broken into two sets. The p_z -orbitals transform as A'_2 and the p_x and p_y pair as E' . Similarly, the d -orbitals are broken into three sets, d_{z^2} , $(d_{x^2-y^2}, d_{xy})$ and (d_{xz}, d_{yz}) . These transform as A'_1 , E' and E'' , respectively. In this case all the orbitals on the central atom have the correct symmetry to form directed bonds.

In the case of Zr, some d -orbitals cannot participate in directed bonding. The three bonds in the basal plane of Zr reduce as $\Gamma_{\sigma}^{\text{equatorial}} = A'_1 + E'$. The bonds normal to the basal plane reduce as $\Gamma_{\sigma}^{\text{axial}} = A'_1 + A'_2$. The s - and p -orbitals can still participate in equatorial and axial bonding, but the (d_{xz}, d_{yz}) pair, which transforms as E'' , cannot. Thus, while the eight valence electrons in Ru will fill all five d -orbitals, the four valence electrons in Zr will occupy the states that give rise to five directed bonds, as the $(d_{xz}$ and $d_{yz})$ character is in states above the Fermi energy (Blaha *et al.*, 1988).

A particularly noticeable feature of the Zr topology is the presence of channels of low charge density perpendicular to the basal plane and passing through the octahedral holes (see Fig. 2). In these channels the region of depleted charge density is considerably extended in comparison to the same channels in Ru (Fig. 1). This is significant because the charge density along these channels will correlate with oxygen solubility.

It has been shown (Eberhart *et al.*, 2005) that the energy of solution can always be expressed as the sum of two terms ΔE_1 and ΔE_2 , which represent the separate changes to the energy of the solute and solvent, respectively. In the case of oxygen solubility the first term, ΔE_1 , is the formation energy of an interstitial oxygen anion from an oxygen atom, and ΔE_2 is the energy change of the metal. In the absence of large lattice reconstructions, ΔE_2 is dominated by the redistribution of metal electrons in response to the anion and ΔE_1 does not vary substantially from one metal to another. Thus, relative oxygen solubility depends on lattice-specific variations of the electron redistribution brought about by an interstitial oxygen atom. In turn, the energy to redistribute metal electrons is derived principally from electrostatics, *i.e.* the work done to embed the oxygen anion in the charge density of the interstitial site. Clearly, the work needed to embed an oxygen interstitial in the charge density around an h.c.p. octahedral hole will be smaller for Zr than Ru.

As we have shown, the topological analysis of the electron charge density provides materials scientists with a tool to develop new structure–property relationships. Here we have reported on the topology of the charge density in two monotonic h.c.p. metals, Ru and Zr, and have demonstrated that there is a relationship between the bonding topologies of these metals and the oxygen solubility.

The result here points to the advantages that would follow from a database of topological structures not unlike current crystal-structure databases. *Acta Crystallographica* Sections C

Table 1

The value of the charge density and principle curvatures at bond CPs in Zr and Ru.

Here ρ_0 is the charge density at the bond CP, λ_3 is the principal curvature parallel to the bond path, and λ_1 and λ_2 are the two principal curvatures perpendicular to the bond path. The density is in $e \text{ \AA}^{-3}$ and the curvatures are in $e \text{ \AA}^{-5}$.

Bond CP	ρ_0	λ_1	λ_2	λ_3
Zr basal plane	0.190	-0.168	-0.080	0.041
Zr out of plane	0.178	-0.139	-0.139	0.114
Ru basal plane	0.363	-0.645	-0.629	2.448
Ru out of plane	0.401	-0.961	-0.754	2.636

and E offer the ideal forum to share the topological structure of solid-state systems with other researchers. The availability of this resource would allow researchers to quickly identify interesting topologies and then investigate the geometry of the corresponding charge density, and when combined with experimental data, to uncover charge-density structure–property relationships.

APPENDIX A

Just as any measurement is subject to experimental error, numerical solutions to the Kohn–Sham equations are characterized by some intrinsic computational error. When it comes to identifying topologies this error will be significant in regions where the charge density is flat, as is the case around the tetrahedral holes of Zr. To be specific, Table 1 compares principal curvatures at the bond CPs in the basal plane of Zr found using *VASP*. It can be seen that the curvature parallel to the bond path in the basal plane, λ_3 , is small. Furthermore, the charge density at these bond CPs is only $1 \times 10^{-3} e \text{ \AA}^{-3}$ lower than that at the pseudo atom. As a result, the topology in this region may be sensitive to the basis set employed in the expansion of the one-electron wavefunctions and to the methods used to calculate the charge density.

To test this possibility, we performed all electron calculations using a linear augmented Slater-type orbital (LASTO) band method (Davenport, 1984), and the *Amsterdam Density Functional Package*, using 68 and 125 atom clusters (de Velde *et al.*, 2001). While the two methods do not capture the same topology around the tetrahedral holes, the Euler characteristic around the holes and behavior of the bond paths away ($\sim 0.1 \text{ \AA}$) from these holes is unchanged. Thus, for ease of discussion, we have chosen the simplest topology that satisfies the Euler characteristic around the tetrahedral holes, that found using *VASP*. If another topology were chosen, however,

the arguments presented here would remain unchanged. It will be interesting to see whether experimental techniques are sufficiently refined to settle the question.

We are grateful to the Defense Advanced Projects Agency and the Office of Naval Research for their support of this research.

References

- Arnold, W. D., Sanders, L. K., McMahon, M. T., Volkov, R. V., Wu, G., Coppens, P., Wilson, S. R., Godbout, N. & Oldfield, E. (2000). *J. Am. Chem. Soc.* **122**, 4708–4717.
- Bader, R. F. W. (1990). *Atoms in Molecules. A Quantum Theory*. Oxford: Clarendon Press.
- Balaha, P., Schwarz, K. & Dederichs, P. H. (1988). *Phys. Rev. B*, **38**, 9368–9374.
- Davenport, J. W. (1984). *Phys. Rev. B*, **29**, 2896–2904.
- Eberhart, M. E. (1996a). *Can. J. Chem.* **74**, 1229–1235.
- Eberhart, M. E. (1996b). *Acta Mater.* **44**, 2495–2504.
- Eberhart, M. E. (2001). *Philos. Mag. B*, **81**, 721–729.
- Eberhart, M. E., Clougherty, D. P. & Louwen, J. N. (1991). *Mater. Res. Bull.* **16**, 53–58.
- Eberhart, M. E., Donovan, M. M. & Outlaw, R. A. (1992). *Phys. Rev. B*, **46**, 12744–12747.
- Eberhart, M. E. & Giamei, A. F. (1998). *Mater. Sci. Eng. A Struct. Mater.* **248**, 287–295.
- Eberhart, M. E., Jones, T. E., Batchelder, M. A. & Olson, G. B. (2005). *J. Mater. Res.* **20**, 1330–1335.
- Farrugia, L. J. & Evans, C. (2005). *J. Phys. Chem. A*, **109**, 8834–8848.
- Hohenberg, P. & Kohn, W. (1964). *Phys. Rev. B*, **136**, 864–871.
- Jones, T. E., Eberhart, M. E. & Clougherty, D. P. (2008). *Phys. Rev. Lett.* **100**, 017208.
- Jones, T. E., Eberhart, M. E., Clougherty, D. P. & Woodward, C. (2008). *Phys. Rev. Lett.* **101**, 085505.
- Kioussis, N., Herbranson, M., Collins, E. & Eberhart, M. E. (2002). *Phys. Rev. Lett.* **88**, 125501.
- Koritsanszky, T. S. & Coppens, P. (2001). *Chem. Rev.* **101**, 1583–1627.
- Kresse, G. & Furthmüller, J. (1996). *Phys. Rev. B*, **54**, 11169–11186.
- Kresse, G. & Joubert, D. (1999). *Phys. Rev. B*, **59**, 1758–1775.
- Luaña, V., Costales, A. & Martín Pendás, A. (1997). *Phys. Rev. B*, **55**, 4297.
- Perdew, J. P., Chevary, J. A., Vosko, S. H., Jackson, K. A., Pederson, M. R., Singh, D. J. & Fiolhais, C. (1992). *Phys. Rev. B*, **46**, 6671–6687.
- Tecplot (2008). *Tecplot – CFD Post Processing, Plotting, Graphing & Data Visualization Software*, <http://www.tecplot.com/>.
- Velde, G. de, Bickelhaupt, F. M., Baerends, E. J., Guerra, C. F., van Gisbergen, S. J. A., Snijders, J. G. & Ziegler, T. (2001). *J. Comput. Chem.* **22**, 931–967.
- Villars, P. & Calvert, L. D. (1985). *Pearson’s Handbook of Crystallographic Data for Intermetallic Phases*, Vol. 3. Metals Park, Ohio: American Society for Metals.
- Vosko, S. H., Wilk, L. & Nusair, M. (1980). *Can. J. Phys.* **58**, 1200–1211.
- Zou, P. F. & Bader, R. F. W. (1994). *Acta Cryst.* **A50**, 714–725.